Carrier dynamics and erbium sensitization in silicon-rich nitride nanocrystals

R. Li,[1] J. R. Schneck,[2] J. Warga,[1] L. D. Ziegler,[2] and L. Dal Negro[1,a)]
[1]*Department of Electrical and Computer Engineering and Photonics Center, Boston University, Boston, Massachusetts 02215, USA*
[2]*Department of Chemistry and Photonics Center, Boston University, 590 Commonwealth Ave, Boston, Massachusetts 02215, USA*

(Received 20 June 2008; accepted 14 August 2008; published online 5 September 2008)

Ultrafast two-color pump-probe measurements, time-resolved photoluminescence (TRPL), and photoluminescence excitation measurements were performed on Si-rich nitride (SRN) and Er doped SRN (Er:SRN) nanocrystals samples. Transient absorption data were compared with picosecond TRPL and excited state absorption cross (ESA) sections σ were measured at different wavelengths. Our data show that σ in Er:SRN, which is approximately 10^{-19} cm^2 at 1.54 μm, does not scale with the $\sim\lambda^2$ behavior predicted by simple free carrier absorption models. Finally, our data demonstrate that in Er:SRN efficient energy transfer to Er ions occurs on the nanosecond time scale with reduced ESA compared to Er-doped oxide-based systems. © *2008 American Institute of Physics*.
[DOI: 10.1063/1.2978069]

Erbium (Er) doping of silicon (Si) based nanostructures is considered a promising approach for the fabrication of light sources suitable for monolithic integration atop the inexpensive silicon electronics platform. Recently, small ($\approx$2 nm in diameter) silicon nanoclusters (Si-ncs) embedded in silicon-rich nitride (SRN) matrices have been shown to yield intense near-infrared light emission with nanosecond dynamics, small temperature quenching, and efficient energy transfer to Er ions.[1–4] In addition, the large effective refractive index of SRN-based light-emitting nanostructured materials enables the fabrication of high quality photonic crystals resonant structures.[5] However, for Er-doped on-chip amplifiers in Si-ncs-based platforms, optical losses due to free carrier absorption (FCA) at 1540 nm must be carefully investigated. In fact, large values of photoinduced absorption cross section $\sigma \approx 10^{-18}$ cm^2 have been reported for oxide-based Er-coupled Si-ncs systems at 800 nm.[6–8] Even higher values can be extrapolated at 1540 nm based on the classical Drude model ($\sigma_{FCA} \sim \lambda^2$) of FCA, severely limiting the maximum optical gain of laser structures. However, a direct measure of photoinduced optical losses at 1540 nm is important in order to unambiguously investigate the nature of the loss mechanisms in Si-ncs systems coupled to Er ions, especially in relation to the novel SRN-based Si-ncs systems (Er:SRN).

In this paper, we report on direct pump-induced optical losses at 1540 nm via two-color pump-probe measurements at different wavelengths in Er-doped Si-ncs embedded in SRN matrices. In addition, by performing time-resolved photoluminescence (TRPL) and photoluminescence excitation (PLE) spectroscopy, we examined the effect of Er incorporation and the dynamics of energy transfer in silicon nitride based nanocrystals.

SRN samples were fabricated on quartz substrates by radio frequency magnetron cosputtering from Si and Si_3N_4 targets. A high density of small Si clusters were formed after postannealing at 700 °C, as discussed in detail elsewhere.[4,9]

Ultrafast pump-probe transient absorption (TA) measurements were performed in the transmission geometry. The output of a titanium sapphire (Ti:Sa) amplifier operated at 100 kHz was used to pump an optical parametric amplifier (OPA). The idler of the OPA was tuned to 1540 nm. Approximately 5% of the amplifier output was frequency doubled to the pump wavelength of 400 nm for both one and two-color measurements. The 800 nm probe beam was split directly from the amplifier. The pump and probe polarizations were set orthogonal to each other. A color filter and an analyzing polarizer were used to minimize the scattered pump. The cross correlation of the pump and the probe was 140 fs. For TRPL experiments, the samples were excited by the second harmonic of a 100 fs pulsed Ti:Sa laser (Mai Tai HP, Spectra Physics) at 430 nm. The TRPL signal was dispersed through a double grating spectrometer (Acton Spectra Pro. 2300i) and detected using a single-photon counting streak camera with 10 ps time resolution (Hamamatsu, C4770). Steady state PL spectra were acquired at room temperature using a 457 nm Ar pump laser (Spectra Physics, 177-602), a photomultiplier tube (Oriel 77348) for SRN emission and an InGaAs detector (Oriel 70368) for the 1540 nm Er emission. The same detectors were also used in PLE experiments together with a xenon lamp (Oriel 6271) selectively filtered by a monochromator (Oriel 74100) within a 10 nm spectral window. All PL spectra have been corrected by the spectral response of the experimental setup. The atomic concentrations of Si, N, and Er in the deposited films were measured, within 0.5% accuracy, by energy dispersive x-ray (EDX) analysis (Oxford ISIS).

We have performed experiments on four SRN-based samples with different Si concentrations: sample A is SRN with 47% Si, sample B is Er:SRN with 47% Si and identical deposition parameters for the SRN matrix as in sample A, sample C is SRN with 55% Si, and sample D is Er:SRN with 49% Si. The Er deposition parameters are identical for all the samples. However, due to the sensitivity limit of the EDX technique, we can only estimate an upper limit of $\approx$1% for the total Er concentration in all the samples.

a)Author to whom correspondence should be addressed. Electronic mail: dalnegro@bu.edu.

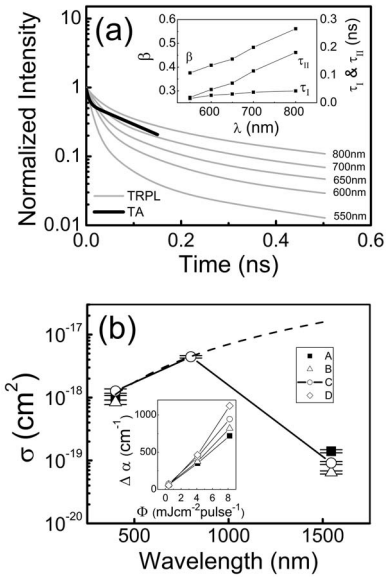

FIG. 1. (a) The PL decays at different wavelengths (gray traces). The solid black line is the TA decay with pump at 400 nm and probe at 1540 nm for sample A. The inset shows the fitting parameters of the sum of a single exponential decay (τ_I) and a stretched exponential decay (τ_{II} and β). (b) The absorption cross section σ obtained with pump at 400 nm and probe at 400 and 1540 nm for samples A, B, and C. Sample C has also been probed at 800 nm. The dash curve is the FCA fit based on the Drude model. The inset shows the linearity of photoinduced absorption change at the pump and probe wavelength of 400 nm for all the samples.

A semilog plot of the normalized instrument response corrected TRPL decays of sample A (gray curves) measured at wavelengths from 550 to 800 nm is shown in Fig. 1(a). As evident in this figure, the decay dynamics of this SRN sample cannot be described by a simple exponential. These emission decays are characterized by two wavelength dependent decay regions; one in the 10–200 ps time regime, the other in the longer 1–50 ns time regime. The subnanosecond TRPL decays [Fig. 1(a)] were best fitted to a sum of a single exponential decay in the shorter time (~10 ps) regime (τ_I) and a stretched exponential decay (τ_{II} and β), capturing the longer time dynamics. The wavelength dependence of the best-fit determined β and τ_I, τ_{II} are shown in the inset of Fig. 1(a). The τ_I fast component is attributed to nonradiative trapping in the system, either in the SRN matrix or within the embedded Si-ncs[10,11]. As for the emission of Si-ncs in silicon oxide matrices, the origin of the stretched decay is a matter of debate[12–15]. However, for small Si-ncs embedded in silicon nitride, we expect that the effects of structural and chemical disorder play an important role. Specifically, Si-ncs nucleate with different sizes, shapes, and can present inhomogeneous surface passivation, typically via N–H related groups,[2,9] when embedded into an amorphous SRN matrix. As a result, an inhomogeneous distribution of radiative states is expected to contribute to the same emission wavelength with different lifetimes, resulting in the observed stretched dynamics. As shown in the inset of Fig. 1(a), τ_{II} and β increase with wavelength. This effect is attributed to energy transfer among Si-ncs. Si-ncs can transfer their energy to neighboring Si-ncs via phonon-assisted transitions, which result in a faster decay rate at shorter wavelengths.[14,16]

All ultrafast pump-probe measurements were performed in the linear excitation regime of the peak photoinduced absorption change, $\Delta\alpha=\alpha(\text{pump on})-\alpha(\text{pump off})$. The linear pump fluence dependence of $\Delta\alpha$ for all the samples is shown in the inset of Fig. 1(b). In addition, the TA decay dynamics are also found to be independent of pump fluence. Thus, nonlinear relaxation processes, such as multielectron Auger recombination, are not significant at these pump fluences. The black line in Fig. 1(a) shows the TA decay curve obtained with 400 nm pump and 1540 nm probe. The TA decay can be fit by a biexponential decay with $\tau_1=5.6$ ps and $\tau_2=146$ ps. Both TA decay time constants (τ_1 and τ_2) occur on a comparable temporal range with the TRPL dynamics [Fig. 1(a)], suggesting that the excited carrier relaxation is responsible for the same dynamics observed in TRPL and TA experiments.

Ultrafast TA experiments are also key to enable direct measurements of the photoinduced absorption cross section σ. The calculated values of σ for the different Si-ncs samples as a function of wavelength are shown in Fig. 1(b). These σ were determined from Beer's law within the small signal regime $\Delta T/T_0 \sim \Delta\alpha d = N^*\sigma d$, where $\Delta T/T_0$ is the measured transient transmission change, $\Delta\alpha$ is the maximum change in the linear absorption coefficient of the material due to the pump pulse, and d is the sample thickness. The number of photoexcited carriers N^* was known by measuring the absorbed pump fluence. This was possible by carefully subtracting, during the pump-probe measurements, the reflected and the transmitted pump signals from the incident one. Assuming the creation of one electron-hole pair per absorbed photon, N^* could be measured and σ extracted at different wavelengths. As shown in Fig. 1(b), the four different Si-ncs samples show similar values of σ at each wavelength. Comparable values of σ have been measured by other groups for porous Si (Refs. 6–8) and Si-ncs embedded in silicon oxide.[17,18] Photoinduced absorption losses in Si-ncs are usually attributed to FCA. Based on either Drude model or quantum theory, the FCA cross section σ increases with wavelength according to a characteristic power-law behavior.[19] The dispersion observed absorption cross sections can be fitted using a $\sim\lambda^2$ scaling only between 400 and 800 nm [Fig. 1(b)]. The observed values of σ at 1540 nm in Er:SRN are about two orders of magnitude smaller than the ones expected by the $\sim\lambda^2$ FCA scaling, and about a factor of 5 smaller than the values reported for Si-ncs in silicon oxide matrices.[17] Our data therefore suggest that the measured photoinduced absorption cannot be explained by simple free carrier processes in Er:SRN samples.

The observed wavelength dependence of σ shown in Fig. 1(b) can be explained by the broad distribution of Si-ncs energy states embedded into the disorder-induced tails of the amorphous SRN matrix. We believe that the 1540 nm absorption probed by TA experiments originates from the excitation of localized transitions within the distribution of energy states corresponding to the Si-ncs dimensions and surfaces passivation, as opposed to FCA absorption.

The observation of smaller σ values at 1540 nm than predicted by the Drude or quantum FCA models in SRN-based nanostructures is important for the engineering of optical amplifiers based on Er energy transfer. The effect of Er incorporation and the dynamics of energy transfer in our samples is discussed in more detail below.

Figure 2(a) shows the PLE spectra measured at 750 nm detection wavelength for sample A (square) and 1540 nm for sample B (triangle). The complete overlap of the two nor-

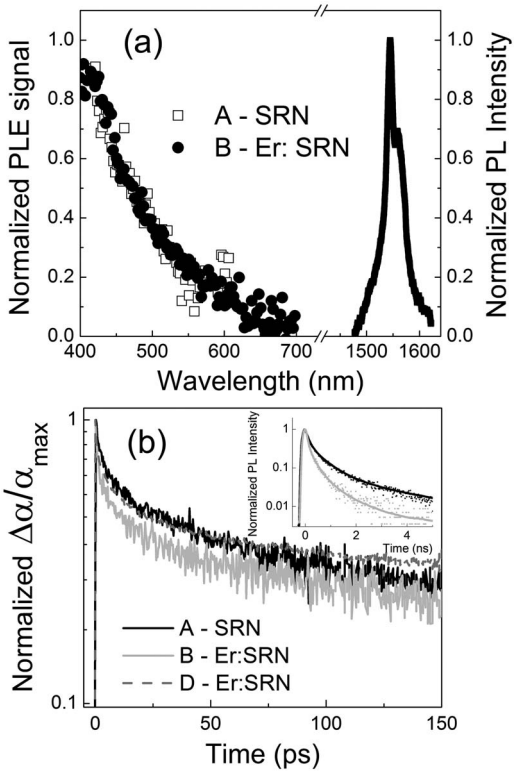

FIG. 2. (a) PLE spectrum with detection wavelength at 750 nm for sample A (square) and PLE spectrum with detection wavelength at 1543 nm for sample B (circle), along with the PL spectrum from sample B. The PL was excited at 457 nm with 5 mW optical power. (b) Normalized TA decays with probe at 1540 nm for sample A and B, and at 800 nm for sample D. The inset shows the PL decay of sample A and B at 800 nm. The solid lines are the fits to the data using a biexponential model convoluted with the systems response.

malized PLE spectra is clear evidence of energy transfer from Si-ncs to Er ions. The PL spectrum of Er in SRN is also shown in Fig. 2(a). Figure 2(b) displays the 400 nm pump, and 1540 nm probed TA responses of samples A and B. Both samples have the same Si concentrations. As evident in Fig. 2(b), sample B, which contains Er, has a faster initial decay on a picosecond time scale when compared with sample A. Thus, we conclude that the incorporation of Er slightly affects the relaxation rate of the system on the picosecond time scale due to small structural changes in the host matrix, which give rise to nonradiative trap states. However, the TA decays of samples A (without Er) and B (with Er) are virtually identical after approximately 30 ps from the pump pulse excitation. Moreover, for time scales larger than ~40 ps, the TA decay dynamics of sample D is very similar to that of samples A and B, despite having a different Si concentration and the presence of Er [Fig. 1(b)]. These results demonstrate that small (<1%) Er concentrations in SRN matrices do not significantly perturb the structure and the optical quality of the embedding matrix, as probed by the sensitive TA decay dynamics for time scales larger than ~40 ps.

However, as shown in the inset of Fig. 2(b), a significant difference exists when comparing the TRPL at 800 nm for samples A and B measured over a 5 ns time scale. The nanosecond PL component of the Er-doped sample is significantly shorter due to the nonradiative energy transfer from Si-ncs to Er ions. In order to quantify the efficiency of the energy transfer process, we have fitted the TRPL decay data using a biexponential model for simplicity, and compared the longer decay components, which are affected by Er incorporation.[4] By following this procedure, we obtained the values of the long decay components for sample B and A as ~1.1 and 2.6 ns, respectively. Based on these results, we can estimate the maximum transfer rate $w_{tr}=1/\tau_B-1/\tau_A \sim (2\ \text{ns})^{-1}$ and transfer efficiency $1-\tau_B/\tau_A \approx 57\%$ in the Er:SRN system.

In conclusion, ultrafast two-color pump-probe measurements have been performed on SRN and Er:SRN samples and compared with TRPL measurements. The photoinduced absorption cross sections σ were measured at different wavelengths and the results demonstrate that this process is due to excited state absorption as opposed to of FCA in SRN-based nanostructures. In addition, by comparing TA and TRPL decays we show that nanosecond transfer rates with 57% maximum efficiency can be achieved in Er:SRN samples.

This work was partially supported by the U.S. Air Force MURI program on "Electrically-Pumped Silicon-Based Lasers for Chip-Scale Nanophotonic Systems" supervised by Dr. Gernot Pomrenke. L.D.Z. acknowledges the support of NSF (Grant No. CHE-0310497) and the Boston University Photonics Center.

[1] N. M. Park, C. J. Choi, T. Y. Seong, and S. J. Park, Phys. Rev. Lett. **86**, 1355 (2001).
[2] L. Dal Negro, J. H. Yi, L. C. Kimerling, S. Hamel, A. Williamson, and G. Galli, Appl. Phys. Lett. **88**, 183103 (2006).
[3] L. Dal Negro, J. H. Yi, J. Michel, L. C. Kimerling, T.-W. F. Chang, V. Sukhovatkin, and E. H. Sargent, Appl. Phys. Lett. **88**, 233109 (2006).
[4] L. Dal Negro, R. Li, J. Warga, and S. N. Basu, Appl. Phys. Lett. **92**, 181105 (2008).
[5] M. Makarova, V. Sih, J. Warga, R. Li, L. Dal Negro, and J. Vuckovic, Appl. Phys. Lett. **92**, 161107 (2008).
[6] P. Malý, F. Trojánek, J. Kudrna, A. Hospodková, S. Banás, V. Kohlová, J. Valenta, and I. Pelant, Phys. Rev. B **54**, 7929 (1996).
[7] K. Luterová, K. Dohnalová, F. Trojánek, K. Neudert, P. Gilliot, B. Honerlage, P. Malý, and I. Pelant, J. Non-Cryst. Solids **352**, 3041 (2006).
[8] J. von Behren, Y. Kostoulas, K. Burak Üçer, and P. M. Fauchet, J. Non-Cryst. Solids **198**, 957 (1996).
[9] L. Dal Negro, R. Li, J. Warga, S. Yerci, S. Basu, S. Hamel, and G. Galli, in *Silicon Nanophotonics: Basic Principles, Present Status and Perspectives*, edited by L. Khriachtchev (World Scientific, Singapore, 2008).
[10] M. Sykora, L. Mangolini, R. D. Schaller, U. Kortshagen, D. Jurbergs, and V. I. Klimov, Phys. Rev. Lett. **100**, 067401 (2008).
[11] F. Trojánek, K. Neudert, P. Malý, K. Dohnalová, and I. Pelant, J. Appl. Phys. **99**, 116108 (2006).
[12] L. Pavesi and M. Ceschini, Phys. Rev. B **48**, 17625 (1993).
[13] J. Ventura, M. C. do Carmo, and K. P. O'Donnell, J. Appl. Phys. **77**, 323 (1995).
[14] J. Linnros, N. Lalic, A. Galeckas, and V. Grivickas, J. Appl. Phys. **86**, 6128 (1999).
[15] C. Delerue, G. Allan, C. Reynaud, O. Guillois, G. Ledoux, and F. Huisken, Phys. Rev. B **73**, 235318 (2006).
[16] F. Priolo, G. Franzò, D. Pacifici, V. Vinciguerra, F. Iacona, and A. Irrera, J. Appl. Phys. **89**, 264 (2001).
[17] D. Navarro-Urrios, A. Pitanti, N. Daldosso, F. Gourbilleau, R. Rizk, G. Pucker, and L. Pavesi, Appl. Phys. Lett. **92**, 051101 (2008).
[18] M. Forcales, M. J. Smith, and R. G. Elliman, J. Appl. Phys. **100**, 014902 (2006).
[19] P. Y. Yu and M. Cardona, *Fundamentals of Semiconductors* (Springer, Berlin, 1996).